Available online at www.sciencedirect.com
ScienceDirect
Journal of the European Ceramic Society 31 (2011) 1791–1801
www.elsevier.com/locate/jeurceramsoc

Texture and micro-nanostructure of porous silicon oxycarbide glasses prepared from hybrid materials aged in different solvents

Aitana Tamayo [a,b,*], Juan Rubio [b], Fausto Rubio [b], Jose L. Oteo [b], Ralf Riedel [a]

[a] Technische Universität Darmstadt, Institut für Materialwissenschaft, Petersenstrasse 23, D-64287 Darmstadt, Germany
[b] Instituto de Cerámica y Vidrio, CSIC, Madrid, Spain

Received 1 December 2010; received in revised form 15 February 2011; accepted 25 February 2011
Available online 7 April 2011

Abstract

The influence of the aging conditions of the preceramic hybrid material on the microstructure of silicon oxycarbide (SiOC) glasses derived therefrom has been highlighted. The textural and structural properties of the glasses are modified by aging the hybrid precursor in different environments. Three solvents have been employed as aging media to produce macroporous SiOC ceramics with porosities in the range between 30 and 70 vol.%.

It has been concluded that the polarity and chemical characteristics of the solvent plays an important role on the surface characteristics and structure of the obtained SiOC glass. Raman spectroscopy and Small Angle X-ray scattering reveal the presence of different nanodomain sizes depending on the polymeric fraction in the preceramic network. The free carbon phase developed during the hybrid-to-ceramic conversion turn out to have a high influence on the growth of the silica nanodomains and thus on the nanostructure of the obtained ceramic.

Keywords: Glass ceramics; Sol–gel processes; Silicon oxycarbide; Microstructure; Porosity; SAXS

1. Introduction

Technological applications of porous silicon based glasses and ceramics derived from preceramic materials become a determinant factor on the increasing number of patents and applications in this area. Silica gels are of special interest due to the low cost of production and raw materials as well. Porous silicon oxycarbide (SiOC) glass obtained from silicon-based hybrid materials have been traditionally used as catalyst, porous adsorbents or catalytic supports in heterogeneous catalysis. The control of the porosity determines the future applications of the new SiOC materials developed.[1,2]

In general, designing materials with controlled porosity permits the selective access of determined substances into pores. Moreover, their appropriate surface area allows the occurrence of the catalytic processes. The intrinsic characteristics of porous SiOC glasses combine their thermal stability and creep resistance with their specific low density. These materials can be obtained either through preceramic polymer pyrolysis or pyrolysis in inert atmosphere of hybrid materials obtained by the sol–gel method.[3,4]

Most of silicon oxycarbide glasses have been prepared in form of powders or dense glasses. However for different applications, monoliths with a given porosity (random or hierarchical) are compulsory. Controlling the pore structure of silicon oxycarbide glasses is an important aspect of developing advanced materials for applications in catalysis,[5] molecular separations,[6] thermal insulation,[7] reinforcement of light metals,[8] dielectric materials,[9] etc.

Various approaches have been used to obtain porous ceramics and SiOC glasses, including direct blowing,[4] decomposition of a siloxane polymer during pyrolysis,[10] sacrificial organosilane linkages,[11] templates,[12] electrohydrodynamic forming,[13] and others (see for instance Colombo[3] and references therein).

The reaction conditions for the synthesis of the hybrid materials as the precursor of the novel glasses play an important role for the texture and microstructural characteristics of the

* Corresponding author at: Instituto de Cerámica y Vidrio, Kelsen 5, 28049 Madrid, Spain. Tel.: +34 91 735 58 40; fax: +34 91 735 58 43.
E-mail address: aitanath@icv.csic.es (A. Tamayo).

0955-2219/$ – see front matter © 2011 Elsevier Ltd. All rights reserved.
doi:10.1016/j.jeurceramsoc.2011.02.039

derived SiOC glasses.[11,14] Pantano et al.[15,16] studied the effect of the pyrolysis temperature on the porous structure of silicon oxycarbide. The transient porosity developed at temperatures between 400 and 800 °C creates a micropore structure attributed to the decomposition of the preceramic network and evolution of gaseous products generated during the ceramization and mineralization process. With increasing pyrolysis temperature the micropores of the SiOC glass transform to meso- and macropores due to densification phenomena. The addition of fillers is a suitable method to stabilize the mesoporous structure after thermal treatment.[17]

The use of solvents for controlling the materials porosity is another interesting route to obtain sol–gel derived porous glasses and ceramics. Solvents can be used for the extraction of phase-separated gels[18] and also in the regulation of the capillary stresses produced during drying of sol–gel derived materials.[19] Drying liquids whose properties are specifically selected were demonstrated to exert a predicted capillary pressure within the evolving pore structure.[20,21] In this sense, non-polar (n-alkanes), polar (acetone, n-alcohols) and mixtures of such solvents, have been used for modifying pore structures and porosities of silica xerogels. For these materials the use of selected solvents mainly controls the capillary pressure, however for sol–gel derived organic–inorganic hybrid materials the solvents may influence not only the capillary pressure but also the extraction of organic molecules entrapped or weakly bonded to the hybrid structure. Therefore, when using hybrid materials for the synthesis of polymer derived glasses and ceramics such as silicon oxycarbide, the described solvent effect has to be taken into account.

In the present work, we have analyzed the influence of the solvent or liquid phase composition on the aging behavior of preceramic hybrid materials and finally on the structural and textural changes of the SiOC glasses derived therefrom. Depending on the solvent composition we have found the development of different nanodomain and pore size distributions in the SiOC matrix starting from the same preceramic hybrid material.

2. Experimental

Tetraethylorthosilicate (TEOS, Mw = 208.32) and silanol-terminated polydimethylsiloxane (PDMS, Mw = 1750) were homogeneously mixed with iPrOH. H_2O and HCl were also stirred for 10 min with the same amount of iPrOH used in the previous solution. The following volume ratios were applied: H_2O:TEOS = 3, HCl:TEOS = 0.3, iPrOH:TEOS = 6 and the weight ratio of TEOS/PDMS is 1.5. Both solutions were mixed and stirred in a temperature controlled flask at 80 °C for 1 h at 600 rpm. Solvent evaporation is avoided by reflux. After 1 h stirring, the clear solutions are poured into a sealed polypropylene container. Gelation of the hybrid materials occurs after 1 h at room temperature. The aging environment is changed by the addition of acetone (A), iPrOH (I), or n-hexane (H) at different times beyond the time of gelation: 1 h (gelling time), 24 h, 120 h or 240 h. Aged gels were dried at 50 and 120 °C until no weight loss is measured. Subsequently, the dried gels are pyrolysed under nitrogen at 1100 °C and 2 h dwelling time at the maximum temperature. Black porous monoliths were obtained after pyrolysis.

Porosity was measured by mercury intrusion porosimetry using a Micromeritics Autopore II 9215 apparatus. Samples were introduced in the penetrometer in particles ranged from 0.5 to 1 mm and gradual pressure increase was applied from 0.03 to 412 MPa that allows the identification of pores of 100 μm–3.2 nm in diameter. The measurement of the applied pressure and intruded volume allows the calculation of porosity, pore size distribution, bulk and skeletal density and porosity as well as related properties such as permeability and tortuosity of the pores or channels. Fracture surfaces were analyzed in a SEM microscope Zeiss mod DSM 950. Images were acquired at 20 kV.

Raman spectroscopy was carried out in a Renishaw InVia Raman spectrometer equipped with a 514 cm^{-1} laser. Spectra were recorded as the average of 10 scans from 200 to 3000 cm^{-1} and exposure time of 20 s. 520 cm^{-1} band of pure Si was used to calibrate the spectrometer. For Small Angle X-ray characterization, powder samples were spread on a thin silicon wafer (80 μm) and exposed to X-rays (40 kV, 50 mA) for 10 min. To get comparative results of all the samples, transmission experiments were carried out by exposition to low energy X-rays (20 kV, 10 mA) for 30 s. All the SAXS analyses were performed in an Anton Paar SAXSess equipment endowed with a Cu X-ray radiation source.

3. Results

3.1. Carbon content

Table 1 summarizes the carbon content for the hybrid preceramic materials and the corresponding silicon oxycarbide glasses derived therefrom. In all cases, the solvent-extracted hybrids present lower carbon content than that of the non-solvent-extracted reference material. Since the only carbon source is the polymer in the hybrid preceramic material, this

Table 1
Carbon content of the obtained SiOC glasses and their hybrid precursors. The labels A, I and H corresponds to the initials of the added solvents, acetone, isopropanol and n-hexane, respectively. Ref indicates the reference material, which is the material with no extra solvents added.

	Ref	A				I				H			
		1	24	120	240	1	24	120	240	1	24	120	240
% C_{hyb}	21.5	19.8	20.3	20.6	21.0	18.6	18.0	18.7	18.5	20.5	19.8	20.6	21.3
% C_{SiOC}	9.2	10.0	9.3	10.1	9.1	9.1	10.6	10.1	8.0	10.6	10.0	9.9	10.1

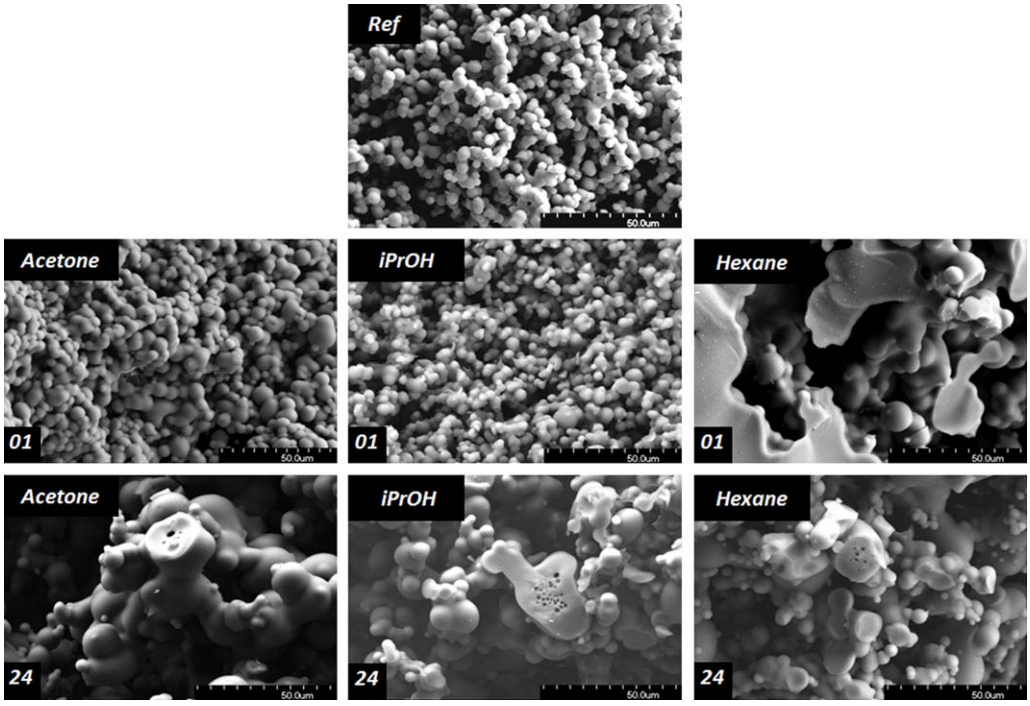

Fig. 1. FEM images of the reference material (up) and the SiOC glasses obtained after the early modification (1 h and 24 h) of the aging aging environment.

result indicates that PDMS molecules non-bonded or entrapped within the network have been removed because of the solvent addition. It is also observed that when the solvent has been added 1 h after gelling, the elimination of PDMS is higher than when added 240 h later, i.e., the extraction capability decreases with the time of solvent addition. This finding is attributed to the reduced contact time of the solvent with PDMS and to the fact that the hybrid structure is more consolidated.

A more pronounced elimination of the polymeric fraction is achieved by using iPrOH followed by acetone, while n-hexane shows a lower extraction capability, indicating that this result is directly related to the polarity of the solvent. The same trend also rules for the obtained SiOC materials where it is observed that the lower carbon contents appear for iPrOH solvent extracted materials, following a series similar to that of the preceramic hybrids. However, although there is no much difference in the total carbon content of the obtained ceramics, the amount of carbon is slightly increased in case of the solvent extraction as compared to the reference material. The higher carbon content of the SiOC materials is discussed in the light that those non-extracted PDMS molecules which remain in the hybrid material are distributed in such a disposition that during the thermal transformation a larger amount of carbon is retained in the glass or ceramic phase. This result clearly indicates that the nanostructure of the derived SiOC materials is not only affected by the presence of different carbon content, but also by the use of solvents to modify the porous texture.

3.2. SEM

Figs. 1 and 2 show the SEM micrographs of the fractured materials obtained after solvent addition at different times. It can be found that each solvent and its respective time of addition result in the formation of different microstructures of the SiOC matrix. In general, all of these materials show morphologies as particulate aggregates with different particle size depending on the type of solvent and of its addition time. Accordingly, the addition of acetone (A) does not produce any change in the microstructure if it is incorporated long time after gelling, while the more pronounced modification occurs for the solvent addition after 1 h (Fig. 1). The addition of iPrOH (I) produces similar microstructural changes as that of acetone, which is in accordance with the fact that both are polar solvents. Aging of the hybrid material in n-hexane (H) shows more significant microstructural modifications for the lowest addition time.

In general, at higher solvent addition times the materials microstructure tends to be similar to that of the reference material. Therefore, it can be pointed out that the alteration of the aging conditions exerts a strong influence on the disposition of the particles due to the penetration of the solvents into the pores and the different interaction with the surface is attributed to their chemical nature. Even at high addition times, when the hybrid material is almost conformed, the exchange of the surface tension inside the pores can modify the final disposition of the particles. When the gel is still fresh, the reaction liquid is filling the pores and voids between the particles. The addition of any solvent at this time produces the modification of the acid–base interactions of the surface of the wet gel with the solvent and hence the polycondensation process. During aging, solvents and reaction liquid are pulled out of the material and the pores become empty. The internal pressure inside the pores is described by the Washburn equation in terms of the surface tension of the filling solvent.[22] Consequently, the change of surface tension induces different capillary pressure inside the pores

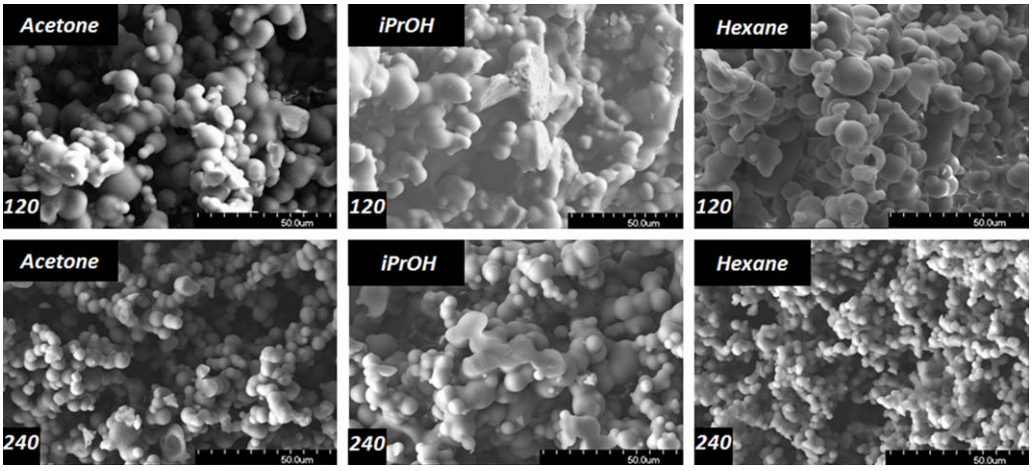

Fig. 2. FEM images of the SiOC ceramics obtained after the late modification (120 h and 240 h) of the aging environment.

which modifies the configuration of the particles in the porous hybrid network. As the inner part of the pores is the last in expel the solvents from inside, the influence of the exchange of the aging conditions becomes more pronounced at high addition times.

When the addition time is increased, the morphology of the SiOC glasses adapt each other for all the solvents (Fig. 2). The microstructure of the SiOC glasses can be preferentially modified in the first stages of the aging step of the hybrid material. When the hybrid network structure is more or less consolidated, it is possible to change the form of the particulate aggregates but not their spheroidal form.

It is also important to notice that the spheroidicity of the aggregates is only modified when non polar solvents are added. The addition of acetone or iPrOH produces always spherical aggregates with different sizes and different conformations depending on the addition time. However, even if the spheroidicity is maintained, interactions between particles in the aggregates modify the pore size and distribution in the bulk material.

3.3. Mercury intrusion porosimetry

In the materials comprised of multiple particle aggregates of micrometric and submicrometric size, the porosity can be

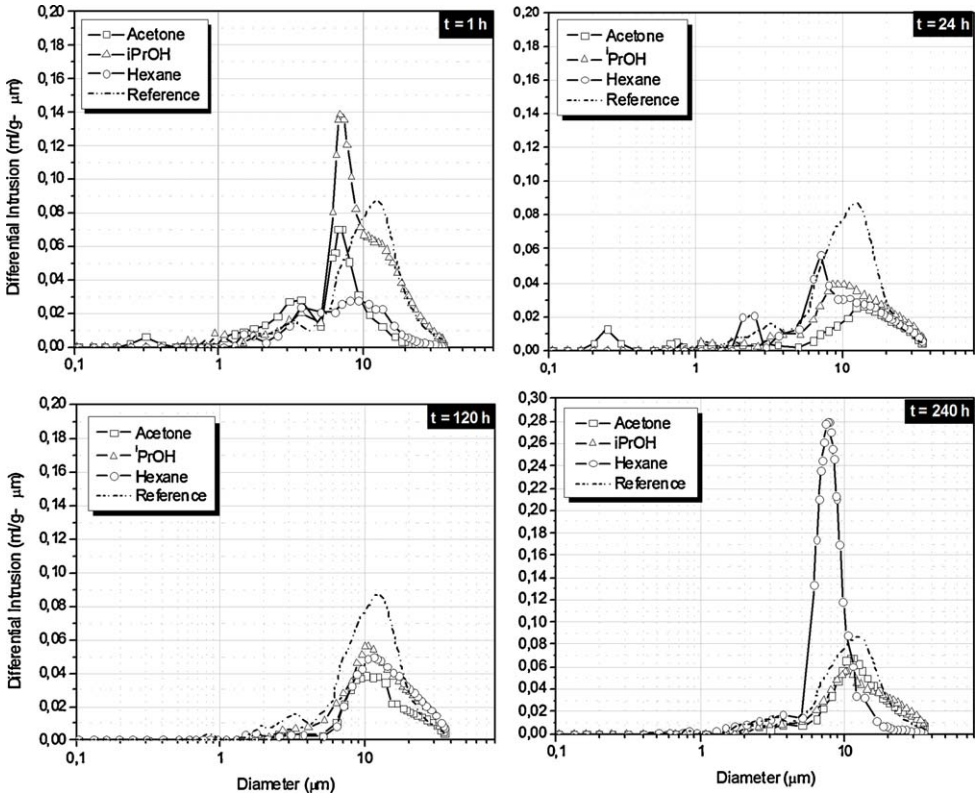

Fig. 3. Pore size distribution for SiOC glasses with different solvents added at different addition times (a) 0d 1 h, (b) 1d, (c) 5d y, (d) 10 days.

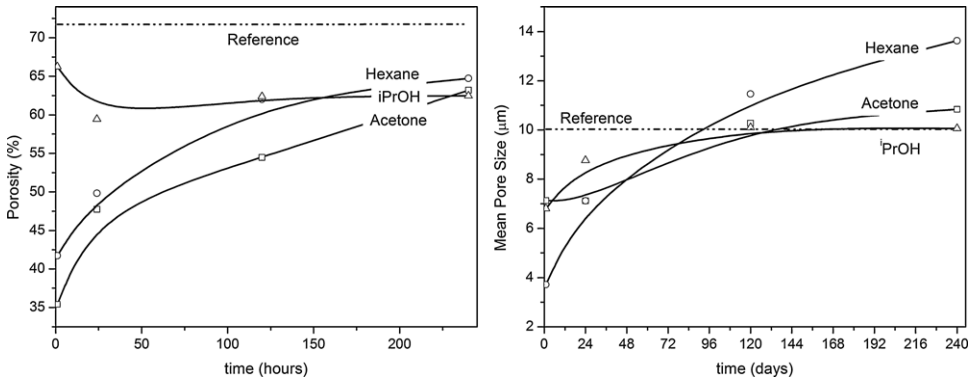

Fig. 4. Evolution of (a) porosity and (b) pore size diameter of SiOC glasses with solvent addition time.

described as voids in the particulate network. These microstructural developments have been analyzed by means of mercury intrusion porosimetry. Pore size distribution curves (PSDs) obtained from those results are represented in Fig. 3. All of these PSD curves can be described as wide distributions with mean pore sizes ranging from 8 to 12 μm. It is found that for addition times of 120 and 240 h, most PSD are quite similar and close to that of the reference material. A narrow and well defined distribution is shown in the case of n-hexane addition after 10 days. These pores with 7 μm in diameter can be originated by some swelling effect in the hybrid network due to the penetration of the n-hexane molecule. However, for low addition times (1 and 24 h) all PSDs show small pores (between 0.5 and 1 μm). Higher differences between different PSD appear for addition time of 1 h, showing that the type of solvent influences the porosity of the hybrid materials network.

Therefore, the decrease of the porosity measured for solvent addition at lower times originates from the reduction of the interparticle gap, which can be due to size homogenization or minor particle size.

Fig. 4 represents the evolution of the textural properties with addition time in terms of porosity and the mean pore size of the SiOC materials that corresponds with the PSD of Fig. 3. In all the studied samples, both porosity and mean pore size increase with addition time, however since porosities of the solvent-added samples are always lower than that of the reference material, mean pore sizes give values above and below of the reference material depending on the addition time. The reference material has an intrinsic porosity of 72%, while in the case of any solvent addition, the porosity hardly reaches 65% when solvent is added after 240 h from gelling time. At lower addition time the porosity of SiOC ceramics acquires values of 35–40% as in the case of acetone or n-hexane addition (non polar or aprotic solvents). It was found that in the case of iPrOH addition, the porosity remains practically constant around 61% at all addition times.

At the same time, it has been analyzed that the mean pore size trend is also influenced by the solvent addition time. For addition times of 1 and 24 h, the typical value of mean pore size is lower than that in the reference material, and for addition times of 240 h those values are found to be higher. These results, together with the porosity values, confirm that the physicochemical characteristics of the solvents used during aging of the preceramic material and their addition time strongly influence the textural properties of the SiOC materials.

In addition to the observed changes in PSD, mean pore size and porosity, the tortuosity data also provide information about the materials texture. Tortuosity can be described as the ratio of the distance travelled between two points to the minimum distance between the same points, and is affected by the packing of former particles. Besides porosity and mean pore size, tortuosity of bulk material is an important feature which allows the characterization of the ability to fluids flowing. It is directly related with permeability. For same pore size and porosity, the material with the higher tortuosity will present the higher resistance to fluids flow. Fig. 5a shows the tortuosity values obtained for the different SiOC materials analyzed in this work. The calculated

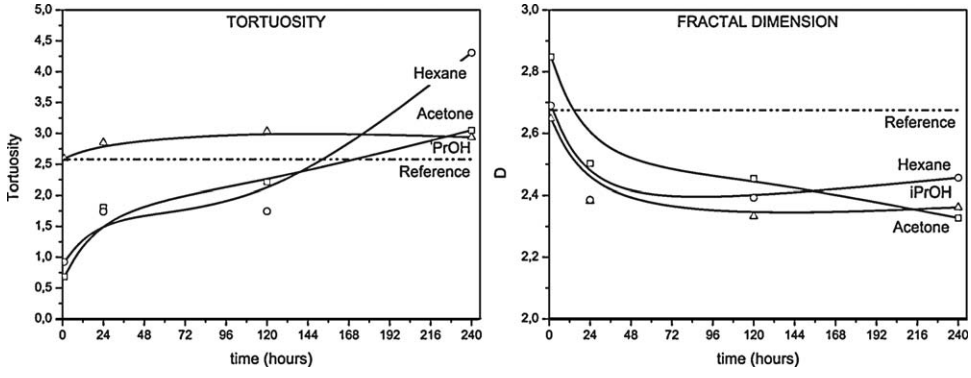

Fig. 5. Tortuosity and fractal dimension of SiOC glasses vs addition time of the solvents.

value of the tortuosity of the reference material is close to 2.5 and this value increases to 3 after addition of iPrOH at different times. Since the pore diameter is found to be of the same order as the reference material, the slight increase in the tortuosity found in the materials where iPrOH was added to the aging environment suggest a decrease in the particle spheroidicity or the formation of surface heterogeneities.

When the gel is still fresh the addition of non polar and aprotic solvents, n-hexane and acetone, reduces the tortuosity of the porous material to values close to 1, which is the minimum value for tortuous materials. When the addition time increases, the effect of the addition of either n-hexane or acetone is increasing this property and the particulate disposition remains unaltered with respect to the reference material. It can be also seen in Fig. 5a that the tortuosity curve trends are similar to the graphs presented in Fig. 4, i.e. the tortuosity depends on both porosity and pore size of the studied material.

Extended information of the textural characteristics is obtained through the reduction of the mercury intrusion porosimetry experimental data in terms of particulate disposition in the bulk material. From the slope of the linear zone in the log P–log V representation, we can obtain the fractal dimension of the pore structure. The fractal dimension D of a solid is a parameter that characterizes the degree of roughness of its surface.[22] The fractal dimension close to 3 represents a rough surface and an increase in the surface area of the particulate whereas fractal dimension approaching to 2 evidences smooth surfaces and less interferences during fluid fluxing.[22] Fig. 5b shows the fractal dimensions of the studied SiOC materials. It is analyzed that the reference material presents a fractal dimension close to 2.7. At lower addition times fractal dimensions of the SiOC materials are also found close to that value, but when increasing the addition time this dimension is reduced independently of the type of added solvent. This fact is interpreted as a softening of the particulate surface because of the effect of changing the aging media.

3.4. SAXS

In addition to the above described textural characteristics, the effect of the solvent addition on the nanostructure of the SiOC glass has been studied through spectroscopic and scattering techniques. SAXS provides information about the aggregates that conforms the amorphous structure over a wide range of length scales typically ranging from one nanometer to about one hundred nanometers. SAXS has been widely used for the structural characterization of a wide range of materials including ceramics, polymers, sol–gel and colloidal systems.[23–27] Fig. 6 shows an example of the SAXS scattering curves of those materials where the solvent has been added after 120 h after the hybrid network synthesis.

The scattered intensity is plotted as a function of the scattering angle (θ) by $q = (4\pi/\lambda)\sin 2\theta$. The atomic structure factor in the X-ray diffraction is equal to the square of the number of electrons in an atom at low angles while the intensity of the scattering is proportional to the number of the scatters in the irradiated volume. In a log–log scale, two main features are found in Small

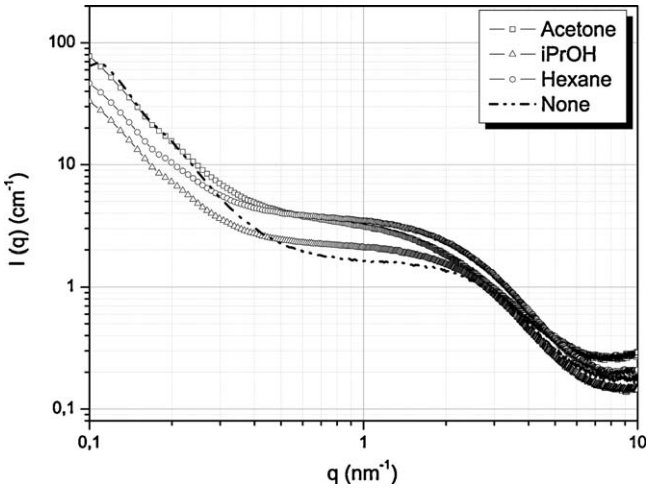

Fig. 6. SAXS curve of the SiOC after addition of the solvents at 120 h.

Angle X-ray scattering diagrams. At high q or Porod regime, the scattered intensity is related with the scattering angle by means of Eq. (1)

$$I(q) = Bq^{-4} \qquad B = I_e 2\pi\rho_e^2 S \tag{1}$$

where S is the average surface area of the primary particle, ρ_e is the average electron density and I_e is the Thompson cross-section of the electron.

Fig. 7 shows the changes induced by the different solvent addition time on the surface area of the primary particle calculated through the Porod approximation in the large q value region. It is analyzed that the samples with iPrOH as the solvent added during the aging period after the synthesis of the preceramic material exhibit a smaller surface area of the primary particles in all cases, even with higher solvent addition times. This finding is in contrast to other solvents which tend to acquire the same value as the preceramic gel is aged in its own liquor. In the case of addition of acetone, a slight increase occurs

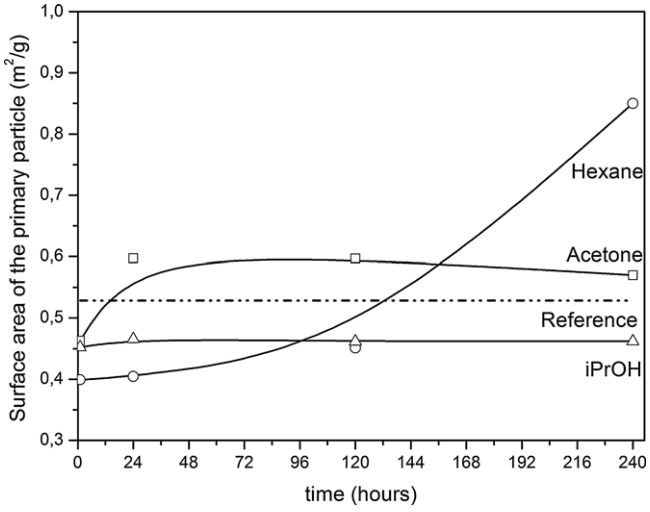

Fig. 7. Surface area of the primary particle vs addition time of the solvents. Note that the reference material is the SiOC material obtained with no solvent addition during aging and drying period.

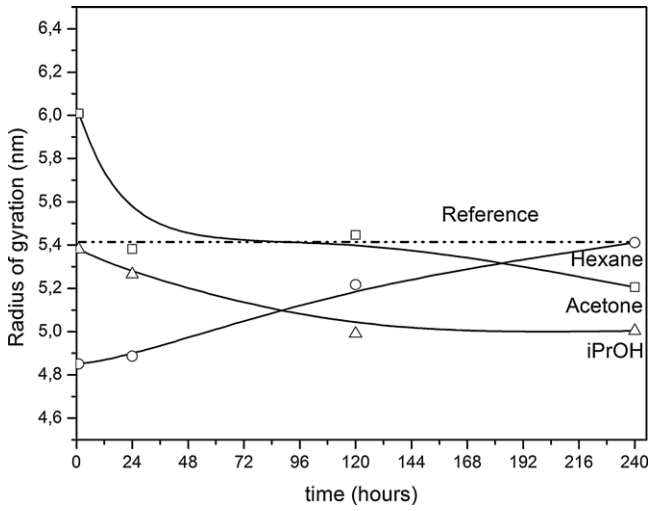

Fig. 8. Radius of gyration of the scatters obtained from the fitting of SAXS curves vs addition time of solvents. Note that reference material is the obtained SiOC ceramic with no solvent addition during aging and drying period.

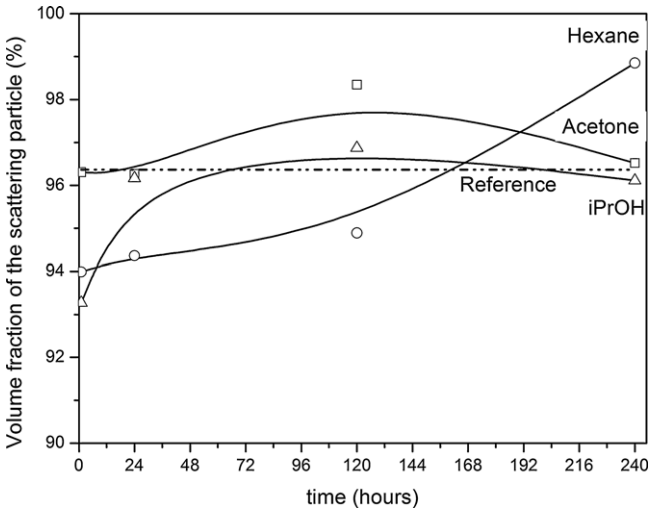

Fig. 9. Volume fraction of the primary particle obtained through the SAXS analysis as a function of the solvent addition time.

with respect to the reference sample when the solvent is added after 24 and 120 h, however the addition of n-hexane produces a continuous increase even at higher solvent addition times.

In the log–log plot, the initial slope (Guinier zone) indicates the main size of the aggregates. It is found that the steeper the slope the bigger the particles. The Guinier region reflects the radius of gyration, R_g, which corresponds to the limits of surface scattering at the average primary particle size. The Guinier's Law describes it as shown in Eq. (2)

$$I(q) = G\exp\left(\frac{-qR_g^2}{3}\right) \qquad G = Nr_e^2\rho_e^2V^2 \tag{2}$$

being V the average particle volume and r_e the average electron radius. The radius of gyration of the particles can be calculated from the representation of $log\, I(q)$ vs q^2 and is valid for dilute and monodisperse systems. This value represents the moment of inertia of the particle which employs the electron density rather than the mass as a weighting factor. A population of monodisperse spheres corresponds to the lower surface area for a given particle size and volume. For spheres, the radius of gyration is related to the primary radii of the particle as $r_g = r\sqrt{(3/5)}$.

The results derived from the calculations of the radius of gyration are presented below in Fig. 8. The radius of gyration of primary spheres tends to acquire the same value as the reference material with the increase of addition time except in the case of the materials aged in iPrOH where the size of the primary particle becomes smaller. In the cases of aging in polar solvents (A and I), this parameter decreases with the addition time, while in the case of n-hexane the trend is increasing until the value of the reference material is reached. In any case, under the assumption of spherical or quasi spherical particles, the diameter of the particles falls in the nanometer scale ranging from 13 to 16 nm.

Our results confirm that not only the porosity of SiOC ceramics is modified through the addition of the different solvents but also their nanostructural characteristics. The radius of gyration is directly related with the size of the particles, which is affected by the polarity of the added solvents, and the surface area provides information of the shape and spheroidicity of the scattered particles.

However, both Guinier and Porod approximations take the data from selected regions, by ignoring the rest of the curve in the calculations. Guinier approximation is valid for dilute systems and employs for its calculations the low q values. On the opposite, Porod approximation calculates with the high q region values and is valid for concentrated systems. In the "knee region" both the form factor and structure factor interfere and accurate calculations can be performed from the least-squares fitting of the curves.

The invariant (integrated intensity of the SAXS curve) was calculated by data integration. The invariant is a well-defined constant which contains some instrumental factors that can be cancelled with background correction. Background was corrected by minimum square fitting from the average of at least 10 points at the higher q values in the small angle range (in the so called Porod's region).

$$Q_N = \int q^2\Delta I(q)d(q) \tag{3}$$

On the two phase model of volume fractions f and $(1-f)$, the integrated intensity is directly proportional to the electron density of the scatters and the Thompson cross-section of the electron:

$$Q = 2\pi^2 I_e(\Delta n)^2 f(1-f) \tag{4}$$

The volume fraction of the scatters shown in Fig. 9 increases with addition time for all the solvents, and reveals a similar behavior to the surface area obtained from the Porod approximation (Fig. 7), showing a significant increase with the addition of n-hexane, especially at higher addition times. The volume fraction is found to be higher than 93% in every case, which can be interpreted as high degree of nanostructuring in this type of materials. The non-nanostructured fraction is attributed to domains ranged beyond the nanoscale.

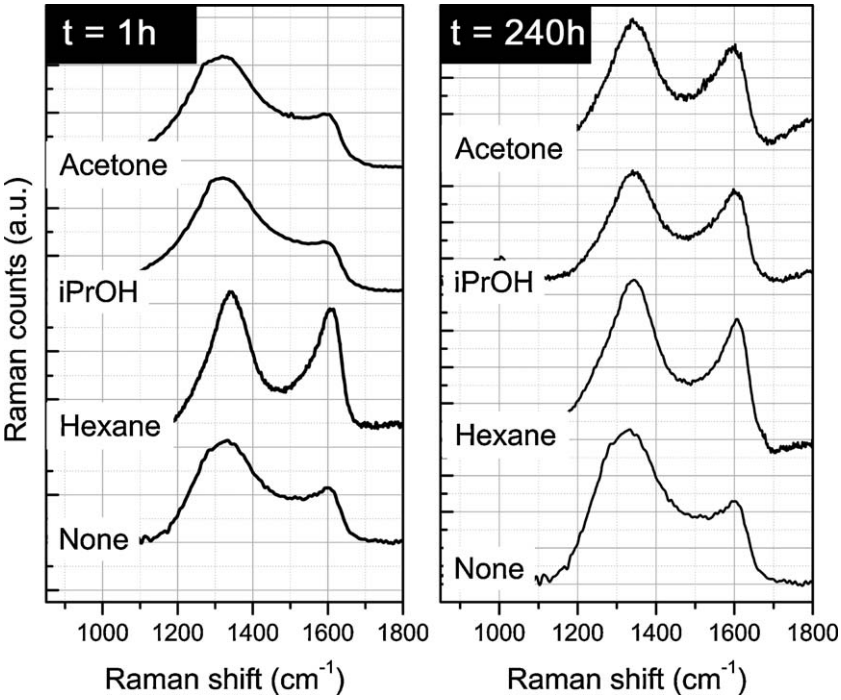

Fig. 10. Raman bands (D and G) of the SiOC obtained through the addition of different solvents at $t = 1$ h and 240 h after geling.

3.5. Raman spectroscopy

It is well known that SiOC materials can be described as a homogeneous distribution of silica, carbon and SiOC nanodomains which conform a glass/ceramic network. These nanodomains shape the nanostructured phases in different conformations. Small Angle X-ray scattering reproduces the scattering of the overall structure which include information of size and shape of the referred domains but this technique does not distinguish between the scattering of the different regions because of the amorphous character. However, Raman spectroscopy informs about the carbon distribution within the glass/ceramic network. Fig. 10 shows some of the obtained Raman curves for the SiOC phase in the specific cases when the solvents have been added after 1 and 240 h after the reaction.

Raman spectroscopy in particular allows the structural characterization of carbon-based materials, and has been used in the last decades to characterize graphitic systems. In our study, the Raman spectra of the synthesized SiOC glasses evidence the presence of carbon due to the appearance of two broad bands centered around 1580 cm^{-1} (G band) and 1340 (D band). The so-called G band is a doubly degenerated phonon mode (E_{2g} symmetry) active for sp^2 carbon networks, and is present in the Raman spectra of all the materials containing sp^2 carbon planar networks. Although the interpretation of the origin of the D band and its relationship with the crystallite size seems not to be clear, the D band has to be associated with defects or edges in the graphite planes. These defects have been related to the sp^3 hybridation of carbon atoms assuming that sp^2 hybridization is still susceptible to continue the graphene layer and do not produce any edge or crystallite defect. Thorough analysis of Raman spectra prove that the G band is accompanied with a weak band, the so called D′ band that is also a disorder-induced Raman feature and centered around 1600 cm^{-1}.[28,29]

The integrated intensity of these bands was obtained by Lorentzian fitting of the spectra. The ratio I_D/I_G has widely used for characterizing the defect quantity in graphite materials since Knight and White[30] related the crystallite size measured by X-ray diffraction with the integrated intensity of D and G bands from the Raman spectra. Several studies have demonstrated the dependence of the D band with the energy of the incident laser due to its dispersive behavior[31,32] but there are still some discrepancies for the dependence of the Raman intensity and crystallite size.[33,34] Recent publications show different trends for crystallite sizes above and below 2 nm that can be fitted in any case by means of laser properties dependent constants.[35] However, it is an agreement in the origin of this vibration mode in terms of a double resonant Raman scattering near the Brillouin zone associated to the presence of lattice defects.[36]

With all of these considerations, we have calculated the L_a value from the ratio of the D and G bands for crystallite size below 2 nm, and the results are shown in Fig. 11. The L_a value for the reference material, or this one with no solvents added during aging and drying, is found to be 1.88 nm and varies with the addition of the mentioned solvents. The addition of any solvent during aging period of the preceramic hybrid material leads to a slight increase of the crystallite size. The trend is an increase in the L_a value from the reference material when n-hexane (non-polar solvent) is added while in the case of the addition of polar solvents such as acetone or iPrOH this effect is exactly the opposite, namely a decrease of L_a with solvent addition time. This behavior follows trend that to the systems acquire the same value than that of the reference material when increasing the solvent addition time. Therefore it is then concluded that

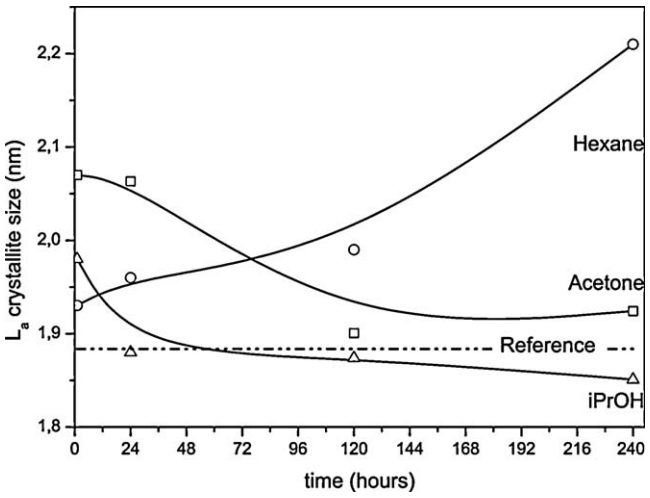

Fig. 11. L_a value of SiOC glasses calculated from Raman spectra vs addition time of solvents.

the carbon redistribution during pyrolysis is strongly affected by the modification of the polarity of the aging environment.

4. Discussion

The above results have shown that the addition of different polar and non-polar solvents to hybrid preceramic materials is a feasible method to modify not only the porous structure of the corresponding SiOC materials, but also their nanostructure over a wide range of length scales. The shape of carbon and silica nanodomains or aggregates directly depends on the selected aging environment.

By adding solvents during the aging period of a hybrid PDMS-silica preceramic material, the capillary force imposed on the network structure is dependent on the liquid–vapor surface tension of the pore fluid and on the angle of contact between the liquid–vapor and solid–liquid interfaces at the pore wall.[37] Then, if different solvents are used, the interactions between the pore fluid and the hybrid material surface are tuned and the pore structure is modified accordingly. However, as it has been outlined in the previous sections, the nanostructure and carbon nanodomains formed out of the SiOC matrix are also modified. These results strongly impose that the type of solvent also influences the PDMS disposition and bonding to the TEOS-derived silica network.

As may be expected, the consequences of the addition of different solvents during the aging period of TEOS-PDMS hybrid materials are found in the sense of stabilizing the hybrid network by elimination of non bonded or weakly bonded PDMS molecules in the hybrid structure. This effect results in a decrease of the carbon content of the hybrid materials with respect to the reference sample, as it has been summarized in Table 1. Moreover, it is well known that during the aging period of TEOS-PDMS hybrid materials, H_2O, solvents, hydrolysis products and non-bonded PDMS molecules are removed from the hybrid structure.[38] These processes lead to specific structures and textures which are changed during the pyrolysis process due to the redistribution-mineralization reactions. These reactions generate a transient porosity when the material is pyrolysed between 400 and 800 °C, which disappear due to sintering phenomena occurring beyond 1000 °C where the material has to be considered as a silicon oxycarbide glass or ceramic.

For hybrid TEOS-PDMS materials it has been suggested that nanometer-scale primary particle growth is governed by hydrolysis and condensation of TEOS. However, micrometer-scale domain growth is due to PDMS involved condensation/polymerization reactions.[39] These inorganic/organic leadership in the nanometer-to-micrometer scales can change along the thermal treatment required to form the SiOC phase. Besides this, microstructural control is also realized by adding different solvents at different times during the aging period of the corresponding pre-ceramic hybrid materials.

At the same time such solvents posses the capability to modify the capillary force of the porous structure. High concentration of low size pores appears when any solvent is added few minutes after gelling (Fig. 3). When the hybrid material has been aged several days in its own solution, its texture is well-consolidated and it is difficult to modify the pore distribution if polar solvents are used. However, if a non-polar solvent like n-hexane is used a swelling effect is found probably due to the interaction of PDMS molecules with that of n-hexane due to their partial solubility. In summary, when the solvents are added at times closer to the gelling point, the more PDMS molecules can be removed and high concentration of low pore sizes is maintained.

An interesting result is that the carbon content of the SiOC glass is higher than in the case of the reference material, despite of the fact that the corresponding hybrids are comprised of lower carbon contents.[21] This feature indicates that the addition of different solvents not only influences the pore structure but also the carbon (or polymer) distribution and the PDMS molecule disposition in the hybrid network. The carbon disposition may alter the redistribution reactions during pyrolysis avoiding the PDMS elimination and thus result in carbon retention in the SiOC structure. In turn, the higher carbon content modifies the nano- and microstructure of the SiOC phase as demonstrated by SAXS analysis.

SAXS studies have shown that higher modifications in the nanometer scale are found when solvents are added after gelling, which also coincides with the longest exposition of the hybrid gel with the aging environment. The non-polar n-hexane gives the lowest radius R_g of the primary particles in the studied SiOC glass or ceramic. The size of the particles increases with the polarity of the solvent, obtaining larger particles when aging in acetone. The effect of n-hexane as aging environment has been also observed in the micrometer scale analyzed by both SEM (Figs. 1 and 2) and mercury intrusion porosimetry (Fig. 3). SEM images show that the typical microstructure composed of micrometer-sized spherical particles of the reference material (Fig. 1) is highly modified when n-hexane is added right after gelling. The particles lose their characteristic spheroidicity and the observed microstructure is not so well-defined. In those SiOC ceramics obtained from the hybrid polymer aged in n-hexane but at higher solvent addition times, the spheroidicity becomes more evident when the period in which the hybrid is aged is reduced (Fig. 2). Some particles of different sizes

Table 2
Characteristic values obtained from the analysis of the mercury intrusion porosimetry curves and SAXS as a function of aging solvent and addition time.

	1 h			24 h			120 h			240 h			Ref
	A	I	H	A	I	H	A	I	H	A	I	H	
Porosity (%)	35.4	66.2	41.7	47.7	59.4	49.9	54.5	62.4	62.0	63.2	62.4	64.7	71.7
Pore diameter (μm)	7.13	6.80	3.71	7.12	8.77	7.12	10.27	10.10	11.47	10.84	10.06	13.63	10.03
Tortuosity	0.68	2.50	0.92	1.80	2.85	1.74	2.21	3.03	1.75	3.05	2.94	4.30	2.58
Fractal dimension	2.85	2.64	2.69	2.50	2.38	2.39	2.45	2.33	2.39	2.32	2.36	2.45	2.67
S (m^2/g)	0.46	0.45	0.53	0.60	0.46	0.40	0.60	0.41	0.45	0.52	0.46	0.85	0.52
R_g (nm)	6.00	5.45	5.47	5.38	5.26	4.88	5.44	4.77	5.21	5.20	5.00	5.41	5.41
$\times 10^{22}$ Q (cm^{-4})	2.46	4.34	2.02	2.48	2.55	3.68	1.12	2.09	3.36	2.32	2.58	7.87	2.42
f (%)	96	93	97	96	96	94	98	97	95	96	96	99	96

are also found, which is correlated with different pore diameters, as found in mercury intrusion porosimetry (Fig. 3). On the other hand, the polar solvents acetone and iPrOH produce similar results in both nanometer and micrometer scales attributed to their polar character. The higher modification is always reached with acetone due to its higher polarity (Table 2).

It has been deduced that when the primary structure is already formed, the addition of the solvent exerts its strong influence in surface processes. In this way, the surface of the particles becomes softer and reduces the interaction between particles, and thus porosity is increased. The modification of surface tension of the aging media also increases the pore diameter because of the pressure variation.

On the nanometer scale, the results obtained by means of Raman spectroscopy are correlated with the results obtained from fitting of the SAXS curves. However, it is important to keep in mind the differences in the results achieved by each technique, namely SAXS and Raman spectroscopy. In the Raman analysis, the information about the carbon phase and graphitic structure is obtained, while the SAXS technique takes into account the scattering produced by heterogeneities on the whole nanometric scale, considering indistinctively carbon, SiOC and pure silica phase. The similarities between the obtained SAXS curves suggest some interrelation between the spectroscopic and scattering results.

Since the radius of the primary scattered particle is higher than the carbon L_a value, we have considered that the carbon nanodomains are included in the scattered primary particle forming a core–shell structure. Thus, silica, carbon and silicon oxycarbide nanodomains result in a kind of nanoheterogeneity. This primary core–shell particle produces the scattering and it is heterogeneously distributed in the amorphous structure of the material. The geometric calculation of the silica domain is presented in Fig. 12 and shows a quasi-linear dependence in all cases. The reference material and the glasses obtained after the addition of acetone lead to silica nanodomains with sizes of ca. 3.5 nm, which is in agreement with the results published by Peña-Alonso et al. for etched SiOC glasses.[40]

Our results suggest that the carbon content and its distribution in the hybrid material, and therefore, the PDMS, plays an important role on the phase development of the SiOC glass. The addition of iPrOH removes the highest amount of PDMS from the hybrid network. The developed carbon nanodomains surrounding the silica particles after pyrolysis are the smallest in size even at high addition times. This fact is attributed to the elimination of the non bonded PDMS exclusively. The elimination of bonded PDMS, together with the pure silica-developing particles, would produce an increase of the silica domains because of the elimination of the carbon-rich phase bonded to silica which acts as a barrier for the coalescence of the SiO_2 domains. This behavior is found for the materials aged in acetone, where the amount of the silica nanodomain is found to be higher than that of the reference material in all cases. On the other hand, n-hexane, which is not able to dissolve PDMS leads to the smallest silica domains but the highest carbon nanodomains, especially at high addition time. Due to the apolar character of this solvent, the PDMS chains adopt coiled configurations which lead to higher carbon-rich aggregates producing the highest amount of carbon nanodomains. The carbon domains effectively hinder the growth of the ceramic silica particles at higher annealing temperatures.

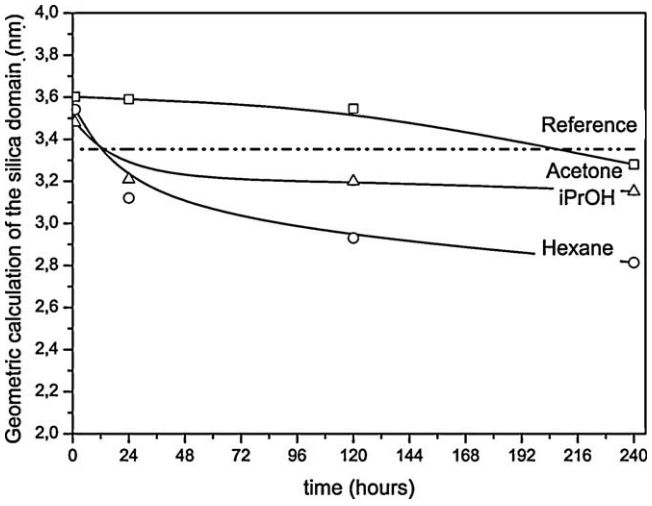

Fig. 12. Geometric calculation of the silica nanodomain size from the combination of Raman and SAXS results.

5. Conclusion

Aging conditions of the preceramic hybrid material have a strong influence on the final compositional and microstructural properties of the obtained SiOC ceramic. The availability of carbon atoms to react during the pyrolysis process determines the

growth of the structural domains and the pore structure. The capillary forces induced in the pores by altering the aging conditions and solvent induce the formation of particles of different sizes and shapes depending on the physico-chemical characteristics of the liquid. In this way, polar solvents lead to the formation of spherical particles, similar to the reference material, but the aggregates lose their specific shape after the addition of n-hexane. Surface smoothness occurs after gelling in different environments which leads to a decrease of the surface fractal constant. In the nanometric scale, the different carbon content and conformation of the polymeric chains in the hybrid material induces the appearance of silica and carbon nanodomains of different sizes. The SAXS results suggest a core–shell type of particles made of carbon, silica and SiOC nanodomains. The largest carbon nanodomains are obtained after aging in n-hexane, while bigger silica domains appear after aging in iPrOH, which is partially soluble in the organic phase of the hybrid polymer.

References

1. Rubio F, Rubio J, Oteo JL. Further insights into the porous structure of TEOS derived silica gels. *J Sol–Gel Sci Technol* 1997;**8**:159–63.
2. Tamayo A, Rubio J, Peña-Alonso R, Rubio F, Oteo JL. Gradient pore size distributions in porous silicon oxycarbide materials. *J Eur Ceram Soc* 2008;**28**:1871–9.
3. Colombo P. Engineering porosity in polymer-derived ceramics. *J Eur Ceram Soc* 2008;**28**:1389–95.
4. Vakifahmetoglu C, Menapace I, Hirsch A, Biasetto L, Hauser R, Riedel R, et al. Highly porous macro- and micro-cellular ceramics from a polysilazane precursor. *Ceram Int* 2009;**35**:3281–90.
5. Liu C, Zhang H, Komarneni S, Pantano CG. Porous silicon oxycarbide glasses from organically modified silica gels of high surface area. *J Sol–Gel Sci Technol* 1994;**1**:141–51.
6. Toury B, Babonneau F. Synthesis of periodic mesoporous organosilica from bis(triethoxysilyl)methane and their pyrolytic conversion into porous SiCO glasses. *J Eur Ceram Soc* 2005;**25**:265–70.
7. Colombo P, Modesti M. Silicon oxycarbide foams from a silicone preceramic polymer and polyurethane. *J Sol–Gel Sci Technol* 1999;**14**:103–11.
8. Zeschky J, Goetz-Neunhoeffer F, Neubauer J, Jason Lo SH, Kummer B, Scheffler M, et al. Preceramic polymer derived cellular ceramics. *Compos Sci Technol* 2003;**63**:2361–70.
9. Valentinotti M, Walter S, Modena S, Sorarù GD. Low dielectric constant porous BN/SiCO made by pyrolysis of filled gels. *J Eur Ceram Soc* 2007;**27**:2529–33.
10. Peña-Alonso R, Téllez L, Tamayo A, Rubio F, Rubio J, Oteo JL. Silicon–titanium oxycarbide glasses as bimodal porous inorganic membranes. *J Eur Ceram Soc* 2007;**27**:969–73.
11. Boury B, Corriu RJP. Adjusting the porosity of a silica-based hybrid material. *Adv Mater* 2000;**12**:989–92.
12. Masse S, Laurent G, Babonneau F. High temperature behavior of periodic mesoporous ethanesilica glasses prepared from a bridged silsesquioxane and a non-ionic triblock copolymer. *J Non-Cryst Solids* 2007;**353**:1109–19.
13. Nangrejo M, Bernardo E, Colombo P, Farook U, Ahmad Z, Stride E, et al. Electrohydrodynamic forming of porous ceramic capsules from a preceramic polymer. *Mater Lett* 2009;**63**:483–5.
14. Cerveau G, Corriu RJP, Framery E, Ghosh S, Mutin HP. Hybrid materials and silica: drastic control of surfaces and porosity of xerogels via ageing temperature, and influence of drying step on polycondensation at silicon. *J Mater Chem* 2002;**12**:3021–6.
15. Singh A, Pantano KCG. Porous silicon oxycarbide glasses. *J Am Ceram Soc* 1996;**79**:2696–704.
16. Pantano CG, Singh AK, Zhang H. Silicon oxycarbide glasses. *J Sol–Gel Sci Technol* 1999;**14**:7–25.
17. Peter G. Active-filler-controlled pyrolysis of preceramic polymers. *J Am Ceram Soc* 1995;**78**:835–48.
18. Whinnery LLL, Nichols MCL, Wheeler DRA, Loy DAA. Process for preparing silicon carbide foam. Albuquerque: N. Sandia Corporation. United States, 5,668,188; 1997.
19. Harreld JH, Ebina T, Tsubo N, Stucky G. Manipulation of pore size distributions in silica and ormosil gels dried under ambient pressure conditions. *J Non-Cryst Solids* 2002;**298**:241–51.
20. Loy DA, Jamison GM, Baugher BM, Russick EM, Assink RA, Prabakar S, et al. Alkylene-bridged polysilsesquioxane aerogels: highly porous hybrid organic-inorganic materials. *J Non-Cryst Solids* 1995;**186**:44–53.
21. Tamayo A, Rubio J. Structure modification by solvent addition into TEOS/PDMS hybrid materials. *J Non-Cryst Solids* 2010;**356**:1742–8.
22. León y León CA. New perspectives in mercury porosimetry. *Adv Colloid Interface Sci* 1998;**76–77**:341–72.
23. Mera G, Tamayo A, Nguyen H, Sen S, Riedel R. Nanodomain structure of carbon-rich silicon carbonitride polymer-derived ceramics. *J Am Ceram Soc* 2009;**93**:1169–75.
24. Glatter O, Kratky O. *Small Angle X-ray Scattering*. London: Academic Press Inc.; 1982.
25. Page R. Applications of small-angle scattering in ceramic research. *J Appl Crystallogr* 1988;**21**:795–804.
26. Shi Y, Wan Y, Zhai Y, Liu R, Meng Y, Tu B, et al. Ordered mesoporous SiOC and SiCN ceramics from atmosphere-assisted in situ transformation. *Chem Mater* 2007;**19**:1761–71.
27. Vollet DR, Donatti DA, Ibañez Ruiz A. A SAXS study of the nanostructural characteristics of TEOS-derived sonogels upon heat treatment up to 1100 °C. *J Non-Cryst Solids* 2002;**306**:11–6.
28. Cançado LG, Jorio A, Pimenta MA. Measuring the absolute Raman cross section of nanographites as a function of laser energy and crystallite size. *Phys Rev B* 2007;**76**:064304.
29. Nemanich RJ, Solin SA. First- and second-order Raman scattering from finite-size crystals of graphite. *Phys Rev B* 1979;**20**:392.
30. Knight DS, White WB. Characterization of diamond films by Raman spectroscopy. *J Mater Res* 1989;**4**:385–93.
31. Pimenta MA, Dresselhaus G, Dresselhaus MS, Cancado LG, Jorio A, Saito R. Studying disorder in graphite-based systems by Raman spectroscopy. *Phys Chem Chem Phys* 2007;**9**:1276–90.
32. Vidano RP, Fischbach DB, Willis LJ, Loehr TM. Observation of Raman band shifting with excitation wavelength for carbons and graphites. *Solid State Commun* 1981;**39**:341–4.
33. Sato K, Saito R, Oyama Y, Jiang J, Cançado LG, Pimenta MA, et al. D-band Raman intensity of graphitic materials as a function of laser energy and crystallite size. *Chem Phys Lett* 2006;**427**:117–21.
34. Ferrari AC, Robertson J. Interpretation of Raman spectra of disordered and amorphous carbon. *Phys Rev B* 2000;**61**:14095.
35. Zickler GA, Smarsly B, Gierlinger N, Peterlik H, Paris O. A reconsideration of the relationship between the crystallite size La of carbons determined by X-ray diffraction and Raman spectroscopy. *Carbon* 2006;**44**:3239–46.
36. Zólyomi V, Kürti J, Grüneis A, Kuzmany H. Origin of the fine structure of the Raman D band in single-wall carbon nanotubes. *Phys Rev Lett* 2003;**90**:157401.
37. Li X, King TA. Spectroscopic studies of sol–gel-derived organically modified silicates. *J Non-Cryst Solids* 1996;**204**:235–42.
38. Mackenzie JD, Chung YJ, Hu Y. Rubbery ormosils and their applications. *J Non-Cryst Solids* 1992;**147–148**:271–9.
39. Guo L, Hyeon-Lee J, Beaucage G. Structural analysis of poly(dimethylsiloxane) modified silica xerogels. *J Non-Cryst Solids* 1999;**243**:61–9.
40. Peña-Alonso R, Sorarù GD, Raj R. Preparation of ultrathin-walled carbon-based nanoporous structures by etching pseudo-amorphous silicon oxycarbide ceramics. *J Am Ceram Soc* 2006;**89**:2473–80.